JACS
JOURNAL OF THE AMERICAN CHEMICAL SOCIETY

ARTICLE

pubs.acs.org/JACS

Pre- and Postfunctionalized Self-Assembled π-Conjugated Fluorescent Organic Nanoparticles for Dual Targeting

Katja Petkau,[†] Adrien Kaeser,[‡] Irén Fischer,[‡] Luc Brunsveld,[*,†] and Albertus P. H. J. Schenning[*,‡]

[†]Laboratory of Chemical Biology and [‡]Laboratory of Functional Organic Materials and Devices, Eindhoven University of Technology, Den Dolech 2, 5612 AZ Eindhoven, The Netherlands

Supporting Information

ABSTRACT: There is currently a high demand for novel approaches to engineer fluorescent nanoparticles with precise surface properties suitable for various applications, including imaging and sensing. To this end, we report a facile and highly reproducible one-step method for generating functionalized fluorescent organic nanoparticles via self-assembly of prefunctionalized π-conjugated oligomers. The engineered design of the nonionic amphiphilic oligomers enables the introduction of different ligands at the extremities of inert ethylene glycol side chains without interfering with the self-assembly process. The intrinsic fluorescence of the nanoparticles permits the measurement of their surface properties and binding to dye-labeled target molecules via Förster resonance energy transfer (FRET). Coassembly of differently functionalized oligomers is also demonstrated, which enables the tuning of ligand composition and density. Furthermore, nanoparticle prefunctionalization has been combined with subsequent postmodification of azide-bearing oligomers via click chemistry. This allows for expanding ligand diversity at two independent stages in the nanoparticle fabrication process. The practicability of the different methods entails greater control over surface functionality. Through labeling with different ligands, selective binding of proteins, bacteria, and functionalized beads to the nanoparticles has been achieved. This, in combination with the absence of unspecific adsorption, clearly demonstrates the broad potential of these nanoparticles for selective targeting and sequestration. Therefore, controlled bifunctionalization of fluorescent π-conjugated oligomer nanoparticles represents a novel approach with high applicability to multitargeted imaging and sensing in biology and medicine.

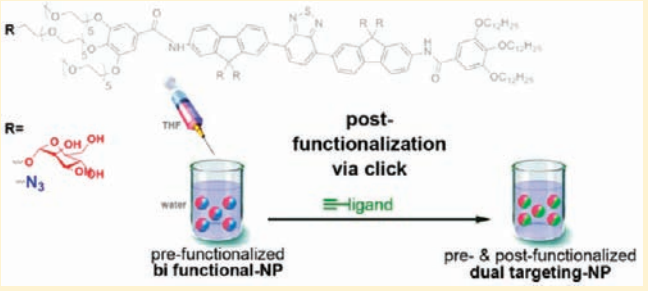

INTRODUCTION

The ability to actively target specific receptors and, as a result, cells is a prerequisite for the use of fluorescent nanoparticles as molecular imaging probes, diagnostics, and therapeutic delivery vehicles.[1] Targeting is typically achieved through surface functionalization of the nanoparticles with high-affinity ligands, such as small molecules, peptides, and antibodies. Multiple ligands can be attached, leading to high binding affinities due to multivalent interactions, which are necessary to achieve maximal selectivity in diagnostics.[2] This at the same time requires chemical control over the ligand functionalization of nanoparticle surfaces via pre- or postfunctionalization.

Several classes of nanoparticles have been developed in the last few decades starting from the first liposomes in the 1960s[3] via inorganic quantum dots[4] to organic nanoparticles.[5] Because of their intrinsic fluorescence with high quantum yields, especially quantum dots are currently widely used as fluorescent imaging probes.[6] Having no intrinsic aqueous solubility, these inorganic nanoparticles require a relatively thick encapsulation layer to ensure biocompatibility and stability. These so-called caps not only solubilize and protect the inorganic core, but as well carry reactive groups, which serve as points of covalent attachment for biomolecules via postfunctionalization.[7] Liposomes, which are based on self-assembled lipid amphiphiles, are prepared from prefunctionalized building blocks.[8] However, sensitive targeting ligands like proteins are attached to liposomes via postfunctionalization.[9] Additionally, in order to construct fluorescent liposomes, dye molecules are introduced, for example, via the polar head groups of the lipids on the outside of the liposome.

Fluorescent organic nanoparticles based on π-conjugated systems combine the features of inorganic nanoparticles and liposomes in being self-assembling amphiphiles with high fluorescence brightness and photostability.[10] The functionalization of these particles with biomolecules, which will be crucial for their use in sensing and imaging applications, has scarcely been reported. π-Conjugated polymer dots have been coassembled with polymers bearing carboxylic acids as attachment points for postfunctionalization by McNeill, Chiu, and co-workers. In this way, the nanoparticle surface was functionalized on the one hand with ethylene glycol chains to provide a biocompatible layer that minimizes nonspecific adsorption and on the other hand with biomolecules to afford specific targeting.[11] Interestingly, these particles were used as probes for in vivo cell labeling and tumor

Received: August 10, 2011
Published: September 13, 2011

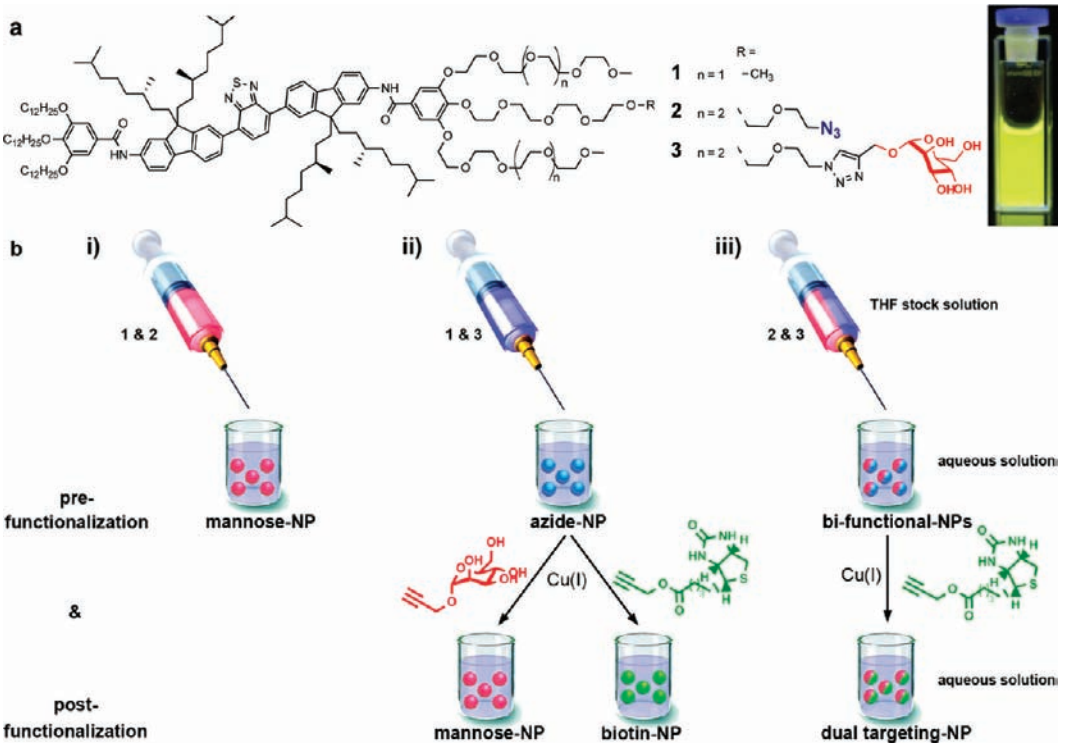

Figure 1. (a) Chemical structures of amphiphiles used in this study and a photograph of a 0.3 μM nanoparticle solution under UV light (360 nm). (b) (i) Generation of nanoparticles prefunctionalized with mannose using mixtures of **1** and **2**. (ii) Generation of nanoparticles prefunctionalized with azides using mixtures of **1** and **3** and subsequent postfunctionalization via copper catalyzed azide−alkyne cycloaddition with alkyne derivatives of either mannose or biotin. (iii) Generation of bifunctional nanoparticles containing azides and mannose using mixtures of **2** and **3** and subsequent postfunctionalization via copper catalyzed azide−alkyne cycloaddition with alkyne derived biotin yielding dual targeting mannose and biotin labeled nanoparticles.

imaging.[11,12] Using a large variation of π-conjugated oligomers, an extensive pioneering structural study has been performed by Lee and co-workers. Mannose prefunctionalized oligomers were designed to assemble into bioactive nanostructures of different shapes showing enhanced binding affinities due to multivalency.[13] Although the nanoparticles were not fluorescent, the encapsulation of a dye was possible, which could even trigger changes in the structure of these dynamic aggregates.[14]

Recently, we have reported on self-assembled fluorescent nanoparticles based on π-conjugated fluorene oligomers in water.[15] Via the coassembly of the different fluorene-based amphiphiles, fluorescent nanoparticles with tunable emission colors covering the entire visible range (including white)[16] were obtained. We now report on a facile and flexible approach to prepare (multi)functional fluorescent organic nanoparticles for (multi)targeted imaging. Via the coassembly of synthetically accessible prefunctionalized π-conjugated oligomers a library of functionalized nanoparticles was generated. The amphiphilic oligomers were on the one hand prefunctionalized with ligands for biological targeting, such as mannose, and on the other hand with azides to allow postfunctionalization of preformed nanoparticles (Figure 1) via the copper-catalyzed azide−alkyne cycloaddition (CuAAC) reaction. Multitargeting of the fluorescent organic nanoparticles was demonstrated through functionalization of the same nanoparticle with different ligands, which were recognized by their corresponding protein partners. The nanoparticles were capable of selective binding to bacteria and to magnetic beads, which led to nanoparticle−target clustering and, in the case of magnetic beads, to complete removal from solution. Our results reveal synthetic pathways and self-assembly protocols to prepare tunable functionalized fluorescent multivalent nanoparticles for biological multitarget imaging applications.

RESULTS AND DISCUSSION

Design and Synthesis. The studied amphiphilic fluorene oligomers **1**−**3** (Scheme 1) consist of the same π-conjugated core of two fluorene units connected by a benzothiadiazole linker. The hydrophobic chromophore has been decorated with gallic acid derivatives bearing at one end alkyl tails and ethylene glycol chains at the other. These hydrophilic ethylene glycol chains are not only necessary for phase segregation but should also prevent unspecific adsorption of biological matter to the surface of the resulting nanoparticles.[17] Furthermore, polyethylene glycols have an excellent water solubility and low toxicity and are now extensively used in clinical applications.[18]

To functionalize the surface of the nanoparticles, our strategy was to introduce ligands at the periphery of hydrophilic ethylene glycol chains. This should ensure the exposure of the ligands to the aqueous environment.[19,20] Two functionalities, a mannose and an azide group, were selected for the prefunctionalization of the oligomers (Figure 1, compounds **2** and **3**, respectively). Mannose is used to evaluate the binding to biological structures such as *Escherichia coli* bacteria[21] and the lectin concanavalin A (ConA),[22] while the

dx.doi.org/10.1021/ja2075345 |*J. Am. Chem. Soc.* 2011, 133, 17063–17071

Scheme 1. Synthesis of the Mannose and Azide Amphiphiles 2 and 3[a]

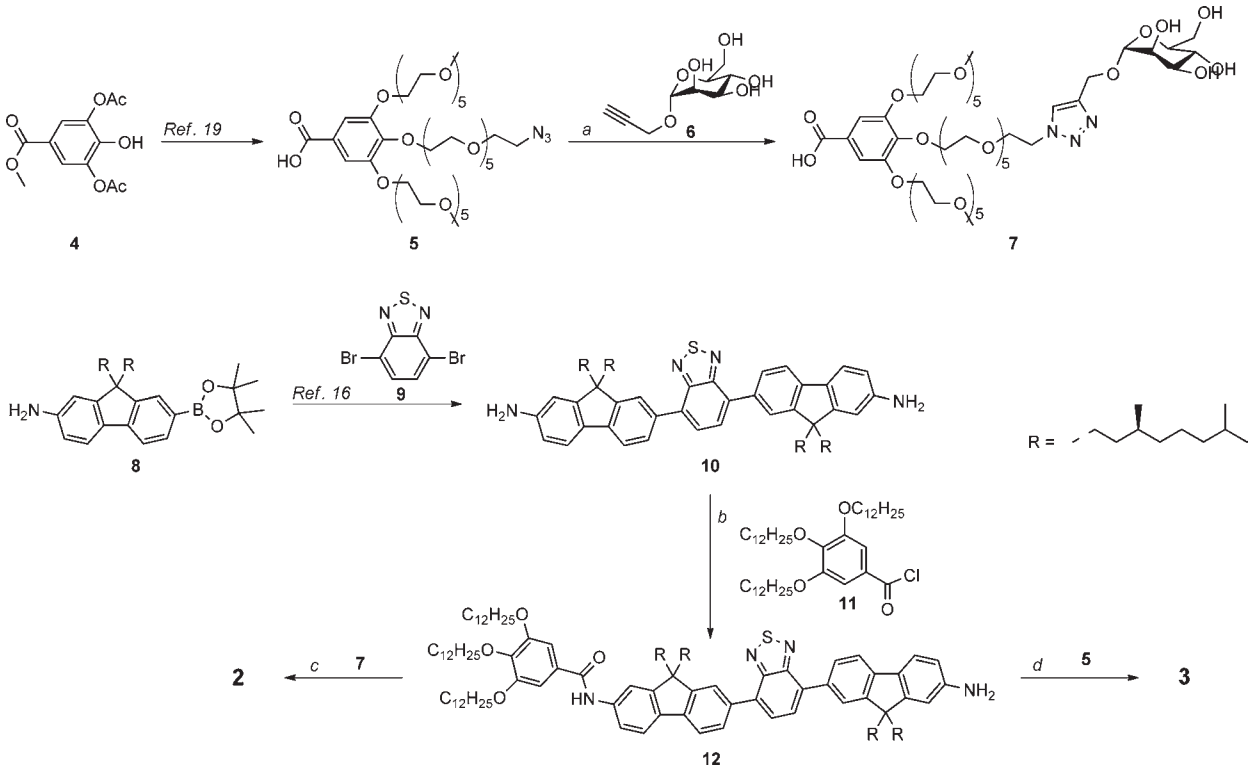

[a] Reagents and conditions: (a) $CuSO_4$, sodium ascorbate, H_2O/tBuOH, 1:1, rt, 56%; (b) Et_3N, CH_2Cl_2, 0 °C to rt, 26%; (c) HBTU, DIPEA, DMF, 40 °C, 47%; (d) (i) $(COCl)_2$, Et_3N, CH_2Cl_2, 0 °C to rt, quant., (ii) Et_3N, CH_2Cl_2, 0 °C to rt, 55%.

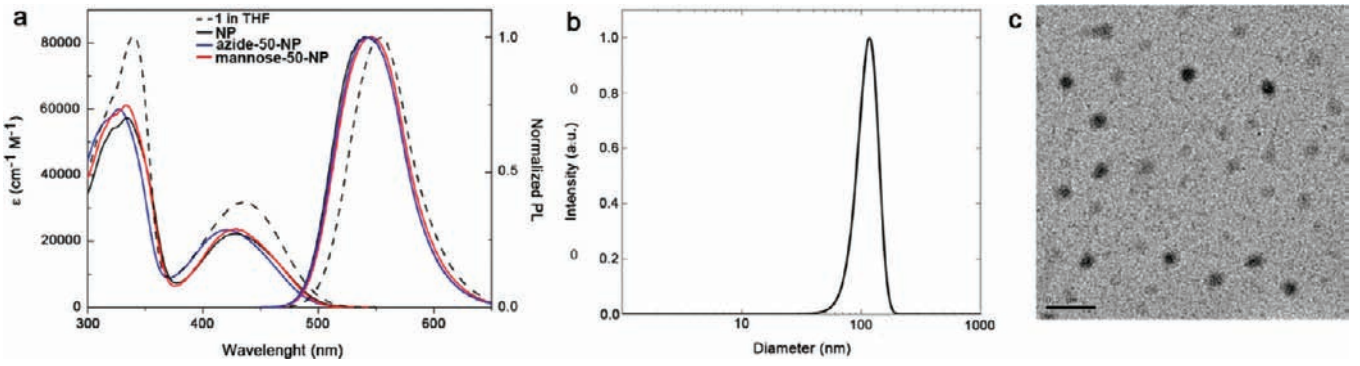

Figure 2. (a) Absorption and emission spectra of self-assembled **NP**, **azide-50-NP**, and **mannose-50-NP** in water and of molecularly dissolved amphiphile **1** in THF (amphiphile concentration for absorption measurement 3 μM, for emission spectra 1.5 μM). (b) Hydrodynamic diameter of **azide-50-NP** (0.3 μM in phosphate buffer) measured by dynamic light scattering. (c) Transmission electron microscopy image of **azide-50-NP**. Scale bar represents 200 nm.

azide moiety allows the preparation of nanoparticles for postfunctionalization via the copper catalyzed azide−alkyne cycloaddition reaction.[23]

The synthesis of amphiphile **1** is based on our earlier reported method.[15] For the synthesis of amphiphile **2** and **3**, the azide-functionalized gallic acid derivative **5** was synthesized in a multistep process, as described previously.[19] Reacting this building block with propargyl mannose **6** in the presence of copper sulfate and sodium ascorbate yielded **7**. Suzuki coupling of benzothiadiazole dibromo compound **9** with aminofluorene boronic ester **8** was followed by acylation of the resulting diamino chromophore **10** with **11**, an acid chloride of gallic acid derivatized with hydrophobic alkyl chains, yielding **12**, which was used for the preparation of functionalized amphiphiles **2** and **3**. For the final acylation step, the azide-functionalized gallic acid derivative **5** was transformed into an acid chloride in situ using oxalyl chloride and reacted with **12**. The mannose-functionalized gallic acid derivative **7** was preactivated using *O*-benzotriazole-*N*,*N*,*N*′,*N*′-tetramethyluronium hexafluorophosphate (HBTU) and subsequently coupled to **12**. Both activation strategies led to the desired amphiphiles. (Scheme 1 and Supporting Information).

dx.doi.org/10.1021/ja2075345 |*J. Am. Chem. Soc.* 2011, 133, 17063–17071

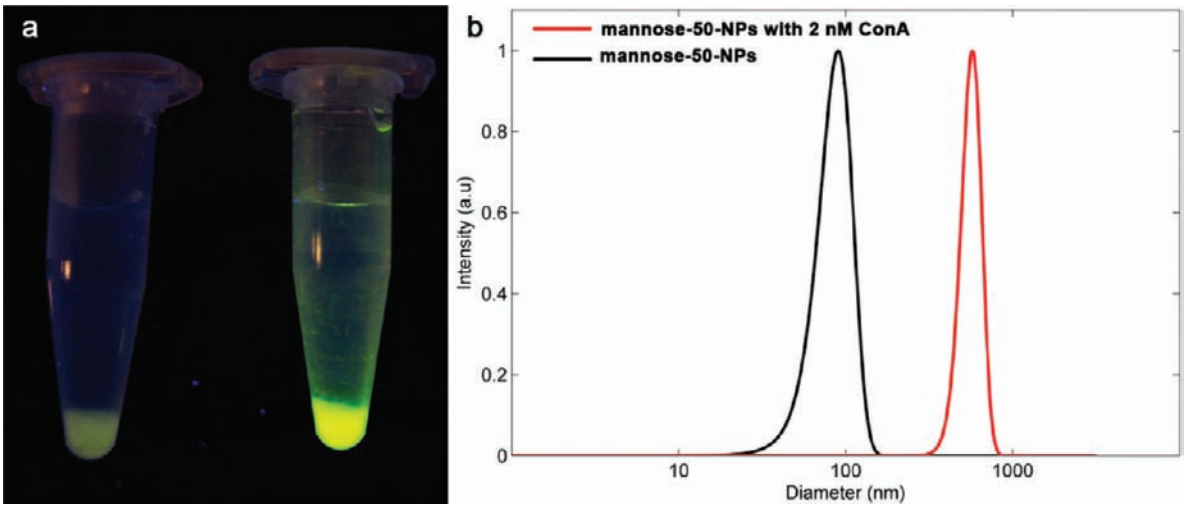

Figure 3. (a) Photograph of washed *E. coli* bacteria under UV illumination after incubation with (left) **azide-50-NP** and (right) **mannose-50-NP** (both 3 μM). (b) Hydrodynamic diameter of **mannose-50-NP**s (0.3 μM) before and after the addition of the lectin ConA (2 nM) measured by dynamic light scattering in phosphate buffer (with 0.1 mM $CaCl_2$ and 0.1 mM $MnCl_2$) at pH = 7.0.

Formation and Characterization of Prefunctionalized Nanoparticles. Nanoparticles from the π-conjugated oligomers were prepared using the reprecipitation method[24] via rapid injection of 15 μL of a 1 mM THF stock solution of the oligomer, or mixtures of oligomers, into 5 mL of water (Figure 1b). In this way, by premixing known volumes of THF stock solutions of the oligomers **1**−**3** before injection, nanoparticles with equal emission colors but different functional group compositions were generated and their properties studied (see also Tables S1 and S2, Supporting Information). Nonfunctionalized nanoparticles (**NP**) of **1** only and functionalized nanoparticles containing 50% of **1** and either 50% of azide amphiphile **3** (**azide-50-NP**) or 50% of mannose amphiphile **2** (**mannose-50-NP**) were also prepared. Dynamic light scattering (DLS) measurements showed for all nanoparticles a similar average hydrodynamic radius of 40−50 nm, which is in good agreement with the size of the spherical nanoparticles observed with transmission electron microscopy (TEM) (Figure 2). The oligomers thus self-assemble into spherical nanoparticles, and the TEM images suggest an amorphous internal morphology. The **NP**, **azide-50-NP**, and **mannose-50-NP** systems all showed identical absorption maxima at around 334 and 430 nm and an emission maximum at 542 nm similar to the previously reported nanoparticles based on self-assembled bolaamphiphilic fluorene benzothiadiazole derivatives[15] (Figure 2a). Additionally, the different nanoparticles all had high quantum yields between 80 and 90% (Tables S1 and S2, Supporting Information). These results show that the introduction of mannose and azide functionalities into the π-conjugated oligomers does not alter the size and optical and fluorescence properties of the nanoparticles. Most likely the self-assembly and optical properties are dominated by the core structure of these amphiphiles, which is not influenced by the introduced functionalities, since these compounds contain the same chromophore, and the hydrophilic/hydrophobic ratio is hardly changed.

To investigate the bioavailability of the introduced mannose, **mannose-50-NP**s were incubated with *E. coli* bacteria, since it is known that mannose specifically binds to the FimH receptor of *E. coli* bacteria.[25] After incubation and washing, the bacterial pellet was yellow fluorescent under UV illumination, showing that the mannose-functionalized particles bind to the bacteria. At the same time, the incubation of *E. coli* with **azide-50-NP** did not stain the bacterial pellet (Figure 3a). Additionally, the hydrodynamic radius of these nanoparticles before and after the addition of mannose binding lectin ConA was measured with DLS (Figure 3b). The addition of ConA to **mannose-50-NP**s significantly increased the hydrodynamic radius of the particles in solution, presumably via the cross-linking of the nanoparticles upon binding to the tetrameric lectin. In contrast, no increase in the size of **azide-50-NP**s was observed via DLS upon addition of ConA (Figure S2, Supporting Information), indicating that the azide functionality does not lead to unspecific binding. Our results show, therefore, that targeting organic nanoparticles can be prepared via a simple coassembly process. Targeting is solely induced through the appending ligand, and unspecific adsorption is prevented by the shielding ethylene glycol chains. At the same time, the introduction of a ligand at the extremities of the π-conjugated oligomers does not affect the optical and self-assembly properties.

Control over Nanoparticle Ligand Density. An important feature of nanoparticles generated via self-assembly of prefunctionalized building blocks should be the facile and reproducible control over ligand density.[26] To investigate the effect of nanoparticle ligand densities on ConA binding, particles containing different amounts of mannose amphiphile were subsequently prepared, ranging from 10% (**mannose-10-NP**) to 90% (**mannose-90-NP**) of **2** (Figure 4a and Supporting Information, Figure S1 and Tables S1 and S2).[27] To determine the influence of ligand density on protein binding, Förster resonance energy transfer (FRET) studies were performed using dye-labeled ConA. Alexa Fluor 633 (AF633) was the dye of choice, as its absorbance spectrum overlaps with the emission spectrum of the nanoparticles. The binding of ConA to mannose on the nanoparticle surface should bring the nanoparticle and the dye-labeled protein in close proximity and enable energy transfer from the fluorene benzothiadiazole donor chromophore to the acceptor dye AF633. Thus, addition of AF633-labeled ConA (ConA-AF633) indeed resulted in a decrease in the emission of **mannose-NP** (λ = 542 nm) and the appearance of AF633 acceptor emission (λ = 648 nm)

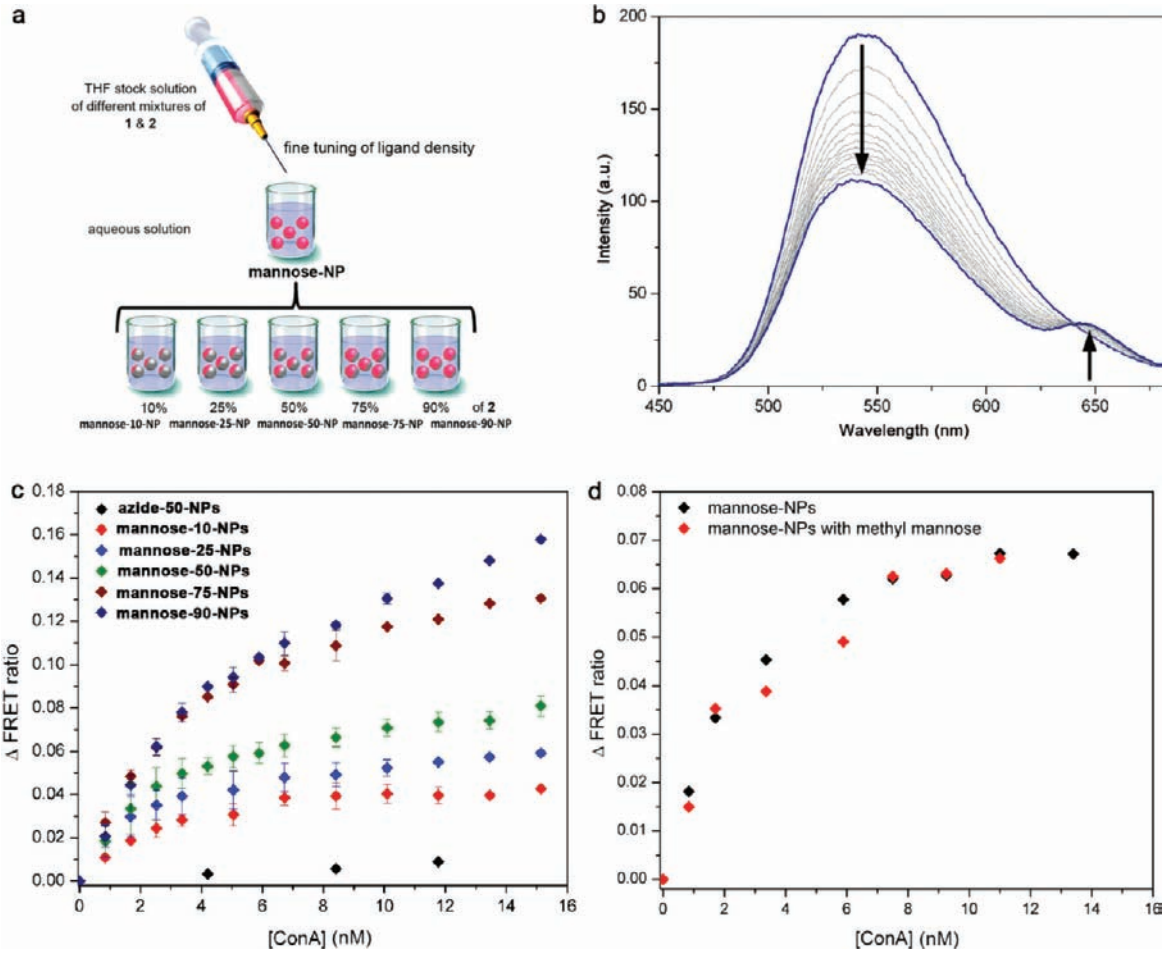

Figure 4. (a) Generation of prefunctionalized mannose nanoparticles with different densities of mannose on the nanoparticle surface using mixtures of **1** and **2**. (b) Change in emission spectra of **mannose-90-NP** upon addition of Alexa Fluor 633 labeled concanavalin A (ConA-AF633; 0.8 −15 nM) caused by energy transfer between nanoparticles and ConA-AF633. (c) Change in FRET ratio of different nanoparticles upon addition of ConA-AF633 shown as the mean value of at least three measurements. The determined nanoparticle−protein energy transfer ratio was constant for different batches of nanoparticles prepared from different stock solutions, underlining the reproducibility of the generated ligand densities. See Figure S3 (Supporting Information) for all titration curves. (d) Change in FRET ratio of **mannose-50-NPs** upon addition of ConA-AF633 without and in the presence of 125 μM methyl mannose. All spectra measured in phosphate buffer (with 0.1 mM $CaCl_2$ and 0.1 mM $MnCl_2$) at pH 7.0 using a nanoparticle concentration of 0.3 μM and an excitation wavelength of 350 nm.

(Figure 4b and Supporting Information, Figure S3).[25] In contrast, when AF633-labeled ConA was added to **azide-50-NP**, no energy transfer was observed, indicating that the mannose molecules attached to the nanoparticles are crucial for binding to ConA (vida supra). Interestingly, a clear correlation between the energy transfer and the percentage of used mannose amphiphile **2** could be observed, with the highest FRET ratio in the case of **mannose-90-NP**s (Figure 4c). A higher mannose density leads to a higher recruitment of proteins to the nanoparticle surface, resulting in an increase in FRET. The tuning of ligand density during the nanoparticle preparation therefore modulates the extent of protein binding to the nanoparticles.

Remarkably, FRET studies in the absence and presence of a 500-fold excess of competing methyl mannose did not lead to changes in FRET ratio (Figure 4d). Methyl mannose is thus not capable of competing with the nanoparticles for ConA binding, showing the strength of lectin ConA binding to the nanoparticles. This indicates that a high ligand density of a low affinity ligand (mannose) leads to increased effective binding affinities of the nanoparticles.[28] This multivalency effect has not been observed for molecular dissolved mannose-containing π-conjugated oligomers[29] and shows the advantage of using self-assembled nanoparticles based on π-conjugated oligomers. The ability to control and tune the ligand density in a single preparation step opens up the possibility to screen for optimal surface functionalization for a given application in a simple and reliable way.

Postfunctionalization via Azide−Alkyne Cycloaddition. Nanoparticles with surface accessible azides enable the introduction of diverse ligands via the copper(I)-catalyzed azide−alkyne cycloaddition (CuAAC) reaction after nanoparticle formation (Figure 1b,ii).[11,30] We have first postfunctionalized the azide nanoparticles, **azide-50-NP**, with mannose to compare the degree of functionalization via the pre- and postfunctionalization methods.

The cycloaddition reaction of azide nanoparticles was performed in degassed water using copper(II) sulfate. The copper salts did not cause any significant quenching of nanoparticle fluorescence (Figure S4, Supporting Information).[11] The excess

of ligand and more importantly the cytotoxic copper salts were removed either by dialysis or PD-10 Sephadex desalting column, both purification methods leading to the same results (Figure S5, Supporting Information). The functionalization was confirmed by mass spectrometry (MALDI-ToF), where, in addition to the mass of the azide amphiphile **3**, the mass of the mannose-functionalized amphiphile **2** could be detected (Figure S6, Supporting Information). After CuAAC functionalization of **azide-50-NP**s with propargyl mannose **6**, changes in the FRET ratio of the postfunctionalized nanoparticles upon addition of ConA-AF633 were measured and correlated with changes in the FRET ratios of prefunctionalized **mannose-50-NP**s. The post-functionalization was successful as observed by the energy transfer from nanoparticle to the dye-labeled protein. When compared with the prefunctionalized **mannose-50-NP**s, the FRET experiments revealed a significantly lower degree of ligand density for the postfunctionalization strategy (Figure 5). On the basis of the observed FRET ratios for the prefunctionalized mannose nanoparticles (Figure 4c), less than 10% of the azide moieties in the **azide-50-NP**s was functionalized with mannose using typical aqueous CuAAC conditions. The lower degree of functionalization via the postfunctionalization method compared with the prefunctionalization is not surprising, as the accessibility and therewith the degree of amphiphile functionalization will be significantly lower for preformed nanoparticles.

Subsequently, biotin was chosen as a second biomolecule to investigate the postfunctionalization of the azide nanoparticles. With a suitable alkyne derivative, biotin could also be successfully introduced onto the nanoparticle surface via CuAAC reaction at room temperature (Figure 1b,ii). The functionalization was

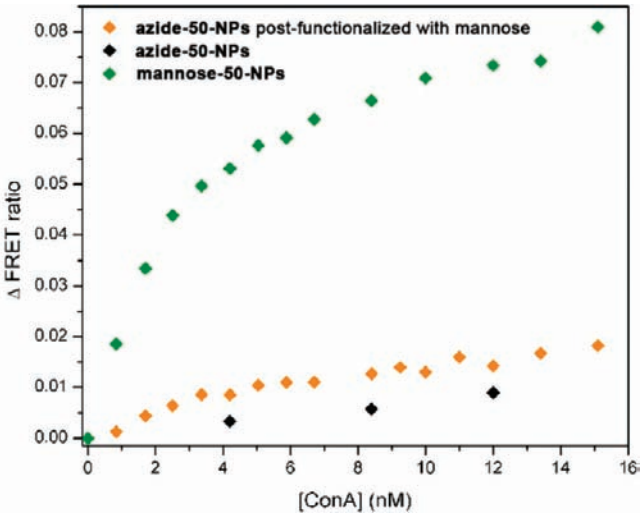

Figure 5. Changes in FRET ratio upon addition of ConA-AF633 to prefunctionalized **mannose-50-NP**s, **azide-50-NP**s, or **azide-50-NP**s postfunctionalized with mannose,[31] in phosphate buffer (with 0.1 mM $CaCl_2$ and 0.1 mM $MnCl_2$) at pH = 7.0 using an excitation wavelength of 350 nm. The nanoparticle concentration was 0.3 μM.

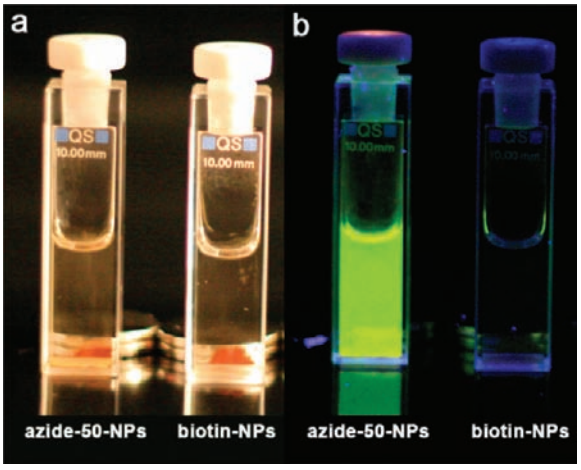

Figure 7. Photographs of **azide-50-NP** and **biotin-NP** under visible light (left) and UV light (right) after incubation with 150 μL of magnetic streptavidin beads (for preparation see the Supporting Information) followed by magnetic separation after 40 min of incubation.

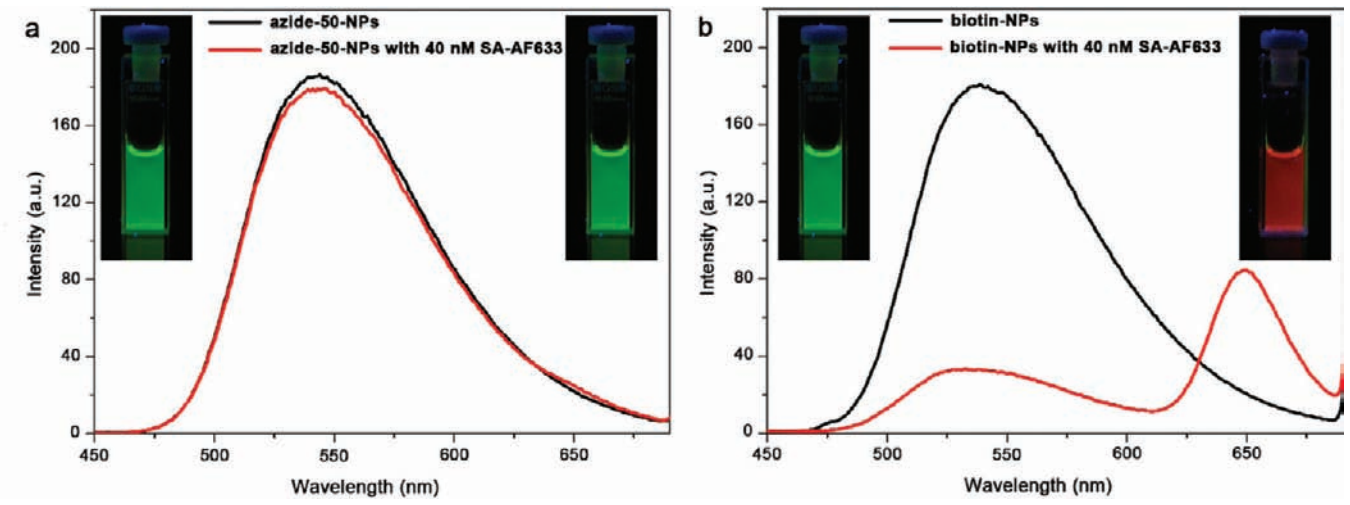

Figure 6. Emission spectra of (a) **azide-50-NP**s and (b) **biotin-NP**s before and after addition of 40 nM Alexa Fluor 633 labeled streptavidin (SA-AF633) showing that only the presence of biotin induces energy transfer. The insets show photographs of the corresponding nanoparticle solutions before (left) and after (right) the addition of 40 nM SA-AF633 under illumination with UV light. Energy transfer from **biotin-NP** to SA-AF633 leads to a strong color change. Spectra were measured in phosphate buffer (with 0.1 mM $CaCl_2$ and 0.1 mM $MnCl_2$) at pH 7.0 using an excitation wavelength of 350 nm. The concentration of nanoparticles was 0.3 μM. See Figure S10 (Supporting Information) for complete titration curves.

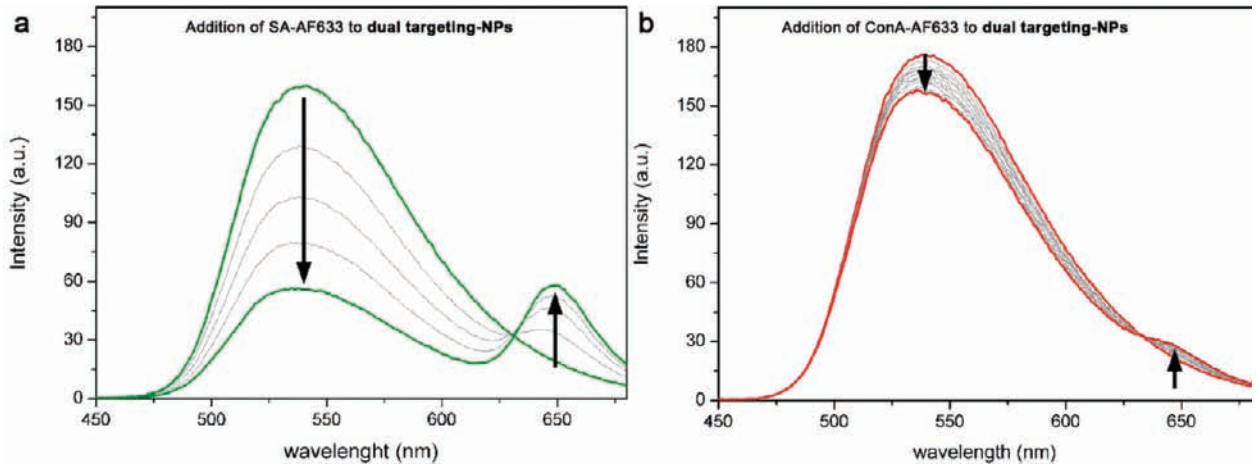

Figure 8. Emission spectra of **dual-targeting-NPs** (0.3 μM), which contain both biotin and mannose upon addition of SA-AF633 (a; 1−5 nM) and of ConA-AF633 (b; 0.8−15 nM) measured in phosphate buffer at pH 7.0 using an excitation wavelength of 350 nm. Energy transfer was observed for both ligands.

confirmed by MALDI-ToF, where both the azide amphiphile **3** and the biotinylated amphiphile were detected. (Figure S7, Supporting Information). Furthermore, DLS and TEM measurements showed no significant changes in the size and shape of the biotin-functionalized nanoparticles (**biotin-NPs**) compared with **azide-50-NP**, as still spherical particles with a somewhat larger hydrodynamic radius of 60 nm were observed (Figure S8, Supporting Information). FRET studies between the postfunctionalized **biotin-NPs** and Alexa Fluor 633 labeled streptavidin (SA-AF633), revealed energy transfer from the fluorene benzothiadiazole donor chromophore to the acceptor dye AF633. No energy-transfer was observed for nonreacted **azide-50-NPs** (Figure 6). The increase in acceptor emission upon binding to the nanoparticles led to a strong color change of the nanoparticle solution when illuminated with UV light, allowing simple optical detection (Figure 6, insets). The addition of the lectin ConA-AF633 did not lead to energy transfer (Figure S9, Supporting Information), suggesting that nonspecific binding does not occur. The energy transfer efficiency was higher for the streptavidin-**biotin-NP** system than for the concanavalin A-**mannose-NP** system (Figure 6 versus Figure 4). This might be explained by the shorter distance between the **biotin-NP** and the Alexa Fluor 633 dye attached to streptavidin, as SA is smaller than ConA and additionally possesses a stronger binding constant to its corresponding ligand.

The isolation of self-assembled postfunctionalized **biotin-NPs** by magnetic streptavidin beads was also investigated.[32] After incubation with these beads and subsequent extraction using a magnet, the solution of **azide-50-NPs** remained fluorescent, suggesting no unspecific binding to the beads. In contrast, the fluorescent **biotin-NPs** were not visible in solution, indicating that the nanoparticles are effectively sequestered from solution (Figure 7).[33] The lack of fluorescence in solution simultaneously underlines the stability of these self-assembled nanoparticles.

This result shows the ability to extract nanoparticles from solution by magnetic beads. This should not only enable the separation of specifically modified nanoparticles in solution but also control circulation times in vivo via an avidin-induced clearance strategy.[34]

Dual-Targeting Nanoparticles. The self-assembly of π-conjugated oligomers enables direct access to bifunctional nanoparticles, which can be used for dual targeting with possible synergistic effects.[35] For this purpose, we combined our pre- and postfunctionalization strategies. First, via self-assembly of prefunctionalized oligomers, **bifunctional-NPs** consisting of 50% mannose-functionalized amphiphile **2** and 50% azide-functionalized amphiphile **3** were prepared (Figure 1b,iii). To evaluate the surface availability of azides for subsequent bioconjugation, the cycloaddition reaction was performed using the alkyne derivative of biotin, yielding mannose- and biotin-containing **dual-targeting-NPs**. The dual targeting properties of these particles were evaluated by measuring the energy transfer between these **dual-targeting-NPs** and both ConA-AF633 and SA-AF633. FRET studies showed that the **dual-targeting-NPs** bind both to ConA and to SA (Figure 8). When compared with the pure **biotin-NPs** and **mannose-50-NPs**, a similar binding behavior was observed (Figure 8 versus Figures 4 and 6), proving the same effective introduction and availability of the targeting ligands. Our results show that a portfolio of pre- and postfunctionalization strategies significantly broadens the flexibility of these nanoparticles in terms of ligand modification and in multitargeting applications.

■ CONCLUSIONS

We have demonstrated facile methods to generate (multi)-targeted fluorescent nanoparticles based on the self-assembly of π−conjugated amphiphilic oligomers in water. Azide and mannose groups were introduced at the periphery of the ethylene glycol chains of the amphiphile. Using these building blocks, a library of differently prefunctionalized nanoparticles was generated. Additionally, the nanoparticle prefunctionalization was combined with subsequent postfuctionalization of azide-bearing nanoparticles via the copper-catalyzed azide−alkyne cycloaddition (CuAAC) reaction, thus expanding the ligand diversity at two independent stages in the nanoparticle fabrication process. The intrinsic fluorescence of these organic nanoparticles enables the simple evaluation of recognition events and surface properties via FRET, showing, for example, their capability and potential for multitargeting. Decoration of nanoparticles with specific ligands induced the selective binding of proteins, bacteria, and magnetic beads to the nanoparticles, which, in combination with the absence

of unspecific adsorption and their stability, proves their broad potential as selective biological targeting tools. The successfully combined pre- and postfunctionalization of fluorescent oligomer nanoparticles represents a novel opportunity to apply these versatile nanoparticles with readily tailored optical properties to imaging applications in biology and medicine.

■ ASSOCIATED CONTENT

Supporting Information. Materials, methods, detailed experimental procedures (synthesis and biological assays), compound characterization, including copies of NMR spectral data and supplementary figures. This material is available free of charge via the Internet at http://pubs.acs.org.

■ AUTHOR INFORMATION

Corresponding Author
a.p.h.j.schenning@tue.nl; l.brunsveld@tue.nl

■ ACKNOWLEDGMENT

We thank Dr. Pol Besenius for help with TEM studies and Ralf Bovee for MALDI-ToF MS measurements. This research has been made possible by a ERC grant 204554—SupraChemBio and The Netherlands Foundation for Scientific Research (NWO) by a VICI grant.

■ REFERENCES

(1) (a) Davis, M. E.; Chen, Z.; Shin, D. M. *Nat. Rev. Drug Discovery* **2008**, *7*, 771–782. (b) Subbiah, R.; Veerapandian, M.; Yun, K. S. *Curr. Med. Chem.* **2010**, *17*, 4559–4577. (c) Shi, J.; Votruba, A. R.; Farokhzad, O. C.; Langer, R. *Nano Lett.* **2010**, *10*, 3223–3230.

(2) (a) Zhou, Y.; Drummond, D. C.; Zou, H.; Hayes, M. E.; Adams, G. P.; Kirpotin, D. B.; Marks, J. D. *J. Mol. Biol.* **2007**, *371*, 934–947. (b) Montet, X.; Funovics, M.; Montet-Abou, K.; Weissleder, R.; Josephson, L. *J. Med. Chem.* **2006**, *49*, 6087–6093.

(3) Bangham, A. D.; Horne, R. W. *J. Mol. Biol.* **1964**, *8*, 660–668.

(4) (a) Medintz, I. L.; Uyeda, H. T.; Goldman, E. R.; Mattoussi, H. *Nat. Mater.* **2005**, *4*, 435–446. (b) Zrazhevskiy, P.; Sena, M.; Gao, X. *Chem. Soc. Rev.* **2010**, *39*, 4326–4354.

(5) (a) Wu, C.; Bull, B.; Szymanski, C.; Christensen, K.; McNeill, J. *ACS Nano* **2008**, *2*, 2415–2423. (b) Tuncel, D.; Demir, H. V. *Nanoscale* **2010**, *2*, 484–494. (c) Pecher, J.; Mecking, S. *Chem. Rev.* **2010**, *110*, 6260–6279.

(6) Biju, V.; Itoh, T.; Ishikawa, M. *Chem. Soc. Rev.* **2010**, *39*, 3031–3056.

(7) Oh, J. K. *J. Mater. Chem.* **2010**, *20*, 8433–8445.

(8) Mulder, W. J. M.; Strijkers, G. J.; van Tilborg, G. A. F.; Cormode, D. P.; Fayad, Z. A.; Nicolay, K. *Acc. Chem. Res.* **2009**, *42*, 904–914.

(9) Strijkers, G. J.; Kluza, E.; Tilborg, G. A. F.; Schaft, D. W. J.; Griffioen, A. W.; Mulder, W. J. M.; Nicolay, K. *Angiogenesis* **2010**, *13*, 161–173.

(10) For some articles on π-conjugated nanoparticles, see: (a) Moon, J. H.; McDaniel, W.; MacLean, P.; Hancock, L. F. *Angew. Chem., Int. Ed.* **2007**, *46*, 8223–8225. (b) Wu, C.; Szymanski, C.; Cain, Z.; McNeill, J. *J. Am. Chem. Soc.* **2007**, *129*, 12904–12905. (c) Kaeser, A.; Schenning, A. P. H. J. *Adv. Mater.* **2010**, *22*, 2985–2997. For reviews and articles about molecularly dissolved π-conjugated polymers and oligomers for imaging and sensing, see:(d) Feng, X.; Liu, L.; Wang, S.; Zhu, D. *Chem. Soc. Rev.* **2010**, *39*, 2411–2419. (e) Herland, A.; Inganäs, O. *Macromol. Rapid Commun.* **2007**, *28*, 1703–1713. (f) Thomas, S. W.; Joly, G. D.; Swager, T. M. *Chem. Rev.* **2007**, *107*, 1339–1386. (g) Xue, C.; Velayudham, S.; Johnson, S.; Saha, R.; Smith, A.; Brewer, W.; Murthy, P.; Bagley, S. T.; Liu, H. *Chem.—Eur. J.* **2009**, *15*, 2289–2295. (h) Duarte, A.; Pu, K.-Y.; Liu, B.; Bazan, G. C. *Chem. Mater.* **2011**, *23*, 501–515. (i) Phillips, R. L.; Kim, I.-B.; Tolbert, L. M.; Bunz, U. H. F. *J. Am. Chem. Soc.* **2008**, *130*, 6952–6954. For reviews on π-conjugated systems with biomolecules to control self-assembly, see:(j) Jatsch, A.; Schillinger, E.-K.; Schmid, S.; Bäuerle, P. *J. Mater. Chem.* **2010**, *20*, 3563–3578. (k) Ruiz-Carretero, A.; Janssen, P. G. A.; Kaeser, A.; Schenning, A. P. H. J. *Chem. Commun.* **2011**, *47*, 4340–4347.

(11) (a) Wu, C.; Schneider, T.; Zeigler, M.; Yu, J.; Schiro, P. G.; Burnham, D. R.; McNeill, J. D.; Chiu, D. T. *J. Am. Chem. Soc.* **2010**, *132*, 15410–15417. (b) Wu, C.; Jin, Y.; Schneider, T.; Burnham, D. R.; Smith, P. B.; Chiu, D. T. *Angew. Chem., Int. Ed.* **2010**, *49*, 9436–9440.

(12) Wu, C.; Hansen, S. J.; Hou, Q.; Yu, J.; Zeigler, M.; Jin, Y.; Burnham, D. R.; McNeill, J. D.; Olson, J. M.; Chiu, D. T. *Angew. Chem., Int. Ed.* **2011**, *50*, 3430–3434.

(13) Kim, B.-S.; Hong, D.-J.; Bae, J.; Lee, M. *J. Am. Chem. Soc.* **2005**, *127*, 16333–16337.

(14) Ryu, J.-H.; Lee, E.; Lim, Y.-beom; Lee, M. *J. Am. Chem. Soc.* **2007**, *129*, 4808–4814.

(15) Abbel, R.; van der Weegen, R.; Meijer, E. W.; Schenning, A. P. H. J. *Chem. Commun.* **2009**, 1697–1699.

(16) Abbel, R.; van der Weegen, R.; Pisula, W.; Surin, M.; Leclère, P.; Lazzaroni, R.; Meijer, E. W.; Schenning, A. P. H. J. *Chem.—Eur. J.* **2009**, *15*, 9737–9746.

(17) Zalipsky, S. *Adv. Drug Delivery Rev.* **1995**, *16*, 157–182.

(18) (a) Caliceti, P.; Veronese, F. M. *Adv. Drug Delivery Rev.* **2003**, *55*, 1261–1277. (b) Karakoti, A. S.; Das, S.; Thevuthasan, S.; Seal, S. *Angew. Chem., Int. Ed.* **2011**, *50*, 1980–1994.

(19) Müller, M. K.; Brunsveld, L. *Angew. Chem., Int. Ed.* **2009**, *48*, 2921–2924.

(20) Ryu, J.-H.; Hong, D.-J.; Lee, M. *Chem. Commun.* **2008**, 1043–1054.

(21) Karlsson, K. A. *Biochem. Soc. Trans.* **1999**, *27*, 471–474.

(22) *Concanavalin A as a tool*, Bittiger, H.; Schnebli, H. P., Ed.; John Wiley & Sons: New York, 1976.

(23) (a) Rostovtsev, V. V.; Green, L. G.; Fokin, V. V.; Sharpless, K. B. *Angew. Chem., Int. Ed.* **2002**, *41*, 2596–2599. (b) Tornøe, C. W.; Christensen, C.; Meldal, M. *J. Org. Chem.* **2002**, *67*, 3057–3064.

(24) Kasai, H.; Nalwa, H. S.; Oikawa, H.; Okada, S.; Matsuda, H.; Minami, N.; Kakuta, A.; Ono, K.; Mukoh, A.; Nakanishi, H. *Jpn. J. Appl. Phys.* **1992**, *31*, L1132–L1134.

(25) Disney, M. D.; Zheng, J.; Swager, T. M.; Seeberger, P. H. *J. Am. Chem. Soc.* **2004**, *126*, 13343–13346.

(26) Gu, F.; Zhang, L.; Teply, B. A.; Mann, N.; Wang, A.; Radovic-Moreno, A. F.; Langer, R.; Farokhzad, O. C. *Proc. Natl. Acad. Sci. U. S. A.* **2008**, *105*, 2586–2591.

(27) DLS and TEM studies revealed aggregation for nanoparticles consisting of pure (100%) **2** only, probably through intermolecular hydrogen bonding of carbohydrates (see ref 10j). Reduction to 90% was found to be enough to overcome unspecific aggregation, as evidenced by DLS.

(28) This strong multivalent binding manifested itself as well during the incubation with *E. coli*, which led to a strong cross-linking of the bacterial pellet.

(29) (a) Kim, I.-K.; Wilson, J. N.; Bunz, U. H. F. *Chem. Commun.* **2005**, 1273–1275. (b) Schmid, S.; Mishra, A.; Bäuerle, P. *Chem. Commun.* **2011**, *47*, 1324–1326.

(30) (a) Cutler, J. I.; Zheng, D.; Xu, X.; Giljohann, D. A.; Mirkin, C. A. *Nano Lett.* **2010**, *10*, 1477–1480. (b) van Dongen, S. F. M.; Nallani, M.; Schoffelen, S.; Cornelissen, J. J. L. M.; Nolte, R. J. M.; van Hest, J. C. M. *Macromol. Rapid Commun.* **2008**, *29*, 321–325.

(31) The figures for postfunctionalized nanoparticles represent typical curves obtained after postfunctionalization. In contrast to reproducible ligand densities achieved via the prefunctionalization approach, the reproducibility of ligand densities via the postfunctionalization approach was less.

(32) Haukanes, B.-I.; Kvam, C. *Nat. Biotechnol.* **1993**, *11*, 60–63.

(33) The intrinsic nanoparticle fluorescence can be used to determine the optimal **biotin-NPs**/magnetic streptavidin beads ratio to

completely remove the nanoparticles from solution (Figure S11, Supporting Information).

(34) Kobayashi, H.; Kawamoto, S.; Star, R. A.; Waldmann, T. A.; Brechbiel, M. W.; Choyke, P. L. *Bioconjugate Chem.* **2003**, *14*, 1044–1047.

(35) Kluza, E.; van der Schaft, D. W. J.; Hautvast, P. A. I.; Mulder, W. J. M.; Mayo, K. H.; Griffioen, A. W.; Strijkers, G. J.; Nicolay, K. *Nano Lett.* **2010**, *10*, 52–58.